Thermochimica Acta, 221 (1993) 85–97
Elsevier Science Publishers B.V., Amsterdam

The kinetics of the compaction at sintering of $MnFe_2O_4$ compressed pellets

E. Segal [a,*], M. Brezeanu [b] and V. Bujoreanu [c]

[a] *Department of Physical Chemistry, Faculty of Chemistry, University of Bucharest, Bulevardul Carol I 13, Bucharest (Romania)*
[b] *Department of Inorganic Chemistry, Faculty of Chemistry, University of Bucharest, Str. Dumbrava Rosie nr. 23, Bucharest (Romania)*
[c] *Department of Metals and Materials Technology, Faculty of Metallurgy and Materials Science, University of Galatz, Str. Domneasca nr. 111, Galatz (Romania)*

(Received 24 September 1992)

Abstract

This paper presents some results concerning the kinetic and mechanistic aspects of the compaction at sintering of compressed pellets of $MnFe_2O_4$.

INTRODUCTION

This work contributes to the understanding of the kinetics and mechanism of the compaction at sintering undergone by pellets formed by compression at 300 and 1000 daN of $MnFe_2O_4$ powders obtained by co-precipitation.

The kinetics of compaction was followed using thermodilatometric (TD), derivative thermodilatometric (TDD) and derivatographic measurements, and X-ray diffraction data.

According to the literature, the spinelic ferrites (particularly $MnFe_2O_4$), and their kinetics of formation and sintering [1–15] have been investigated extensively.

EXPERIMENTAL

Rings of $MnFe_2O_4$ ($9.2 \times 6 \times 5\,mm^3$) were used for the dilatometric measurements; they were formed by bilateral compression at 300 and 1000 daN of $MnFe_2O_4$ powder hand-blended with 2% binder. The other measurements were recorded from powdered samples.

* Corresponding author.

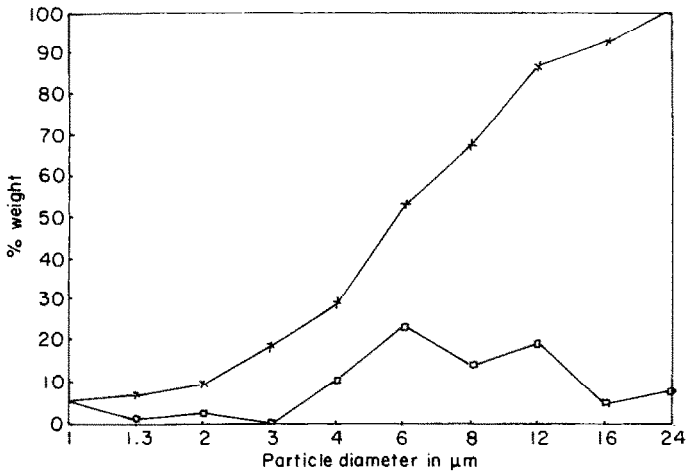

Fig. 1. Granulometric curves of the $MnFe_2O_4$ powder prepared by co-precipitation: ×, integral granulometric curve; □, differential granulometric curve.

The $MnFe_2O_4$ powders exhibited the granulometric composition shown in Fig. 1, as determined using a 'Cilas' granulometer. The heating curves (TG, DTG, DTA and T) were recorded on a MOM (Budapest) Paulik–Paulik–Erdey derivatograph. The derivatograms shown in Fig. 2 were recorded in air, at a heating rate of $10\,K\,min^{-1}$.

The curves showing the change in intensity of the $MnFe_2O_4$ diffraction line with $d = 2.124$ Å ($2\theta = 19.2°$) were recorded on a DRON-3 diffractometer using the Kα radiation of molybdenum, at a heating rate of $25\,K\,min^{-1}$ (Fig. 3). The non-isothermal TD curves (Figs. 4 and 5) and the non-isothermal TDD curve (Fig. 6) were recorded in air at atmospheric pressure, at a heating rate of $5\,K\,min^{-1}$, using Harrop TDA equipment.

The isothermal TD curves (Figs. 7–12) were recorded on the same equipment, the samples being heated at $5\,K\,min^{-1}$ until isothermal conditions were obtained, and then maintained in isothermal conditions for times ranging from 100 to 150 min. The experimental data obtained from Figs. 7–12 were analysed in order to obtain information on the kinetics and mechanism of compaction, using the general equations of mass transport at sintering [2, 3] and the kinetic equations describing the decomposition of solids and the reactions between solids [16, 17].

The degree of compaction was calculated according to

$$\alpha = \frac{\Delta L}{\Delta L_{max}} = \frac{L - L_0}{L_{max} - L_0} \tag{1}$$

where L_0 is the initial height of the sample, L is the height of the sample at time t of the isothermal treatment, and L_{max} is the height of the sample at the end of the isothermal treatment.

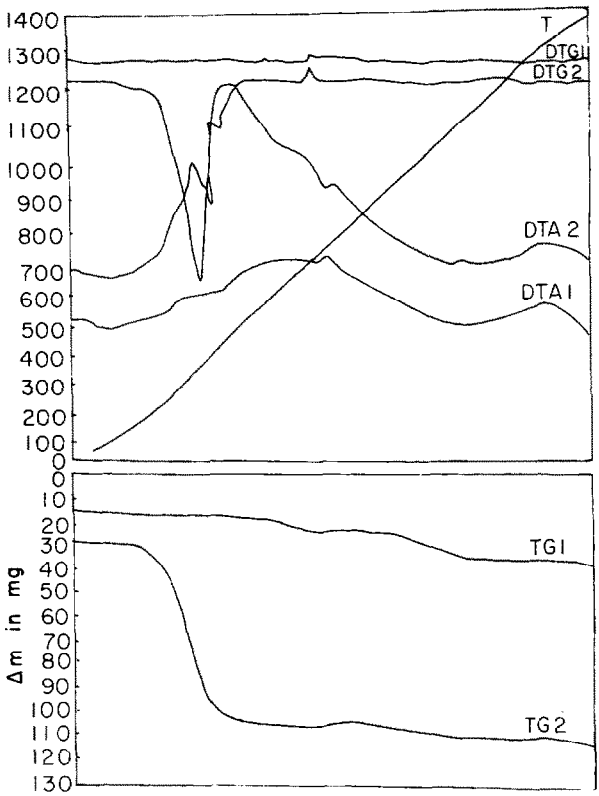

Fig. 2. The derivatograms for: 1, pure powdered $MnFe_2O_4$; and 2, the mixture of $MnFe_2O_4$ powder with binder.

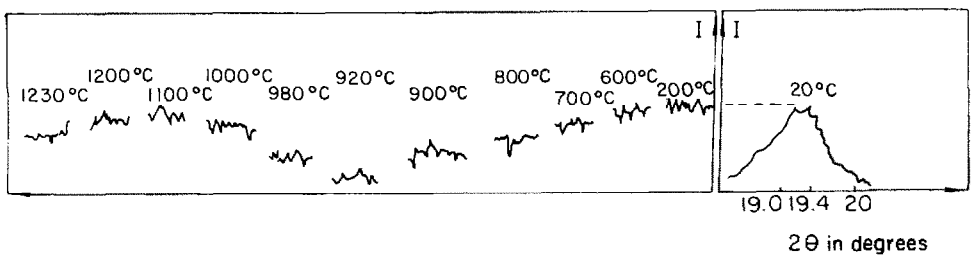

Fig. 3. The change in the $MnFe_2O_4$ powder X-ray diffraction peak ($d = 2.124$ Å) with temperature.

RESULTS AND DISCUSSION

The isothermal dilatometric curves illustrated in Figs. 4 and 5 show that the second step of sintering, the compaction step, occurs approximately in the range 650–1110°C.

The change in the slopes of the TD curves indicates a corresponding

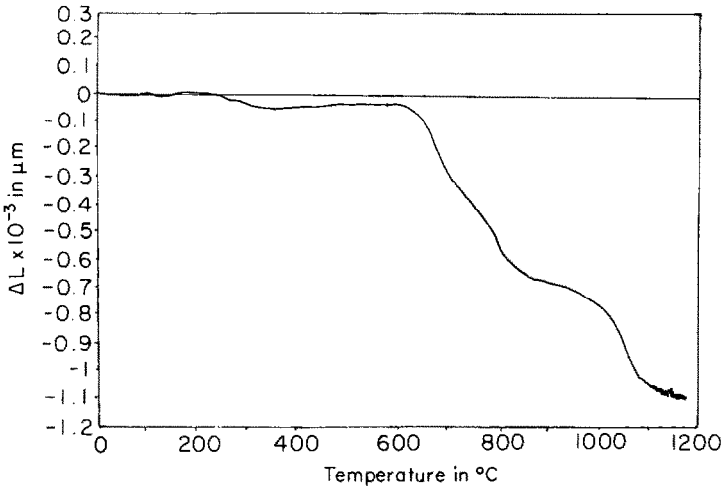

Fig. 4. Experimental TD curve for an $MnFe_2O_4$ sample compressed at 300 daN.

change in the compaction mechanism. At lower temperatures in the above-mentioned range, the decrease in the lattice parameter corresponding to the changes $MnFe_2O_4 \rightarrow \alpha\text{-}Fe_2O_3 + Mn_3O_4$ and $Mn_3O_4 \rightarrow Mn_2O_3$ acts in the same way as the capillary forces facilitating the contraction. In the range 900–1000°C, the contraction is hindered due to the nucleation of the spinelic phase of $MnFe_2O_4$ in the previously formed cubic Mn_3O_4 [8]. For samples compressed at both 300 and 1000 daN, there are three temperature ranges with significant contraction: 650–700, 700–800 and 1000–1100°C.

In the range 100–600°C, the samples compressed at 1000 daN exhibit two

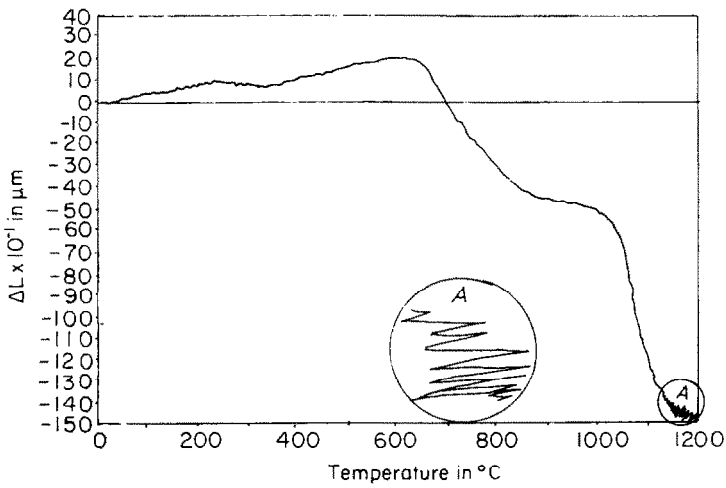

Fig. 5. Experimental TD curve for an $MnFe_2O_4$ sample compressed at 1000 daN.

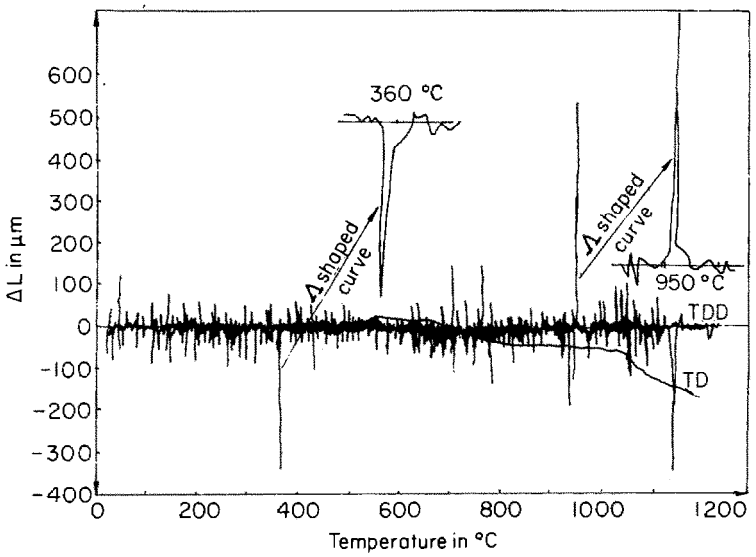

Fig. 6. Experimental TDD curve for an $MnFe_2O_4$ sample compressed at 1000 daN.

dilatation steps (Fig. 5). These can be assigned to the slow diffusion of water and of the gaseous products, resulting from the thermooxidative degradation of the binder, through the material with a higher degree of compaction. These compounds diffuse at a rate lower than the rate of the reactions generating them.

Near 1100°C, the samples undergo melting at the grain boundaries. This can be identified in the TD curve by the detail A in Fig. 5. The melting leads to a sharp change in the dimensions of the samples (Fig. 7a) and to an intensity decrease in the specified diffraction line of $MnFe_2O_4$ (Fig. 3).

The contraction steps no longer occur at 1200°C (Fig. 7b), and a rigid frame is generated on which the magnetic material will recrystallise. Thus, at 1200°C, the sintering of $MnFe_2O_4$ enters the third, final step which ends at 1350°C as shown by the exothermic crystallisation peak on the DTA curve (Fig. 2).

At around 360 and 950°C respectively, the TDD curve (Fig. 6) shows two second-order phase changes (LAMBDA shape changes) which are characteristic of the structural, magnetic changes [18]. These changes, if correlated with the equilibrium diagrams [5, 6] and with the changes in the intensity of the X-ray diffraction line of $MnFe_2O_4$ with $d = 2.123$ Å, can be assigned to the ferri → paramagnetic ($MnFe_2O_4 \rightarrow \alpha$-$Fe_2O_3 + Mn_3O_4$) and tetragonal → cubic ($Mn_2O_3 \rightarrow Mn_3O_4$ and α-$Fe_2O_3 \rightarrow \gamma$-$Fe_2O_3$) changes, respectively.

The isothermal TD curves recorded in the range 650–800°C, when plotted as degree of conversion (α) versus time exhibit a sigmoid form (Figs. 13–15) for $0 < \alpha < 0.7$, which is characteristic for reactions that occur through nucleation and growth of the nuclei [17].

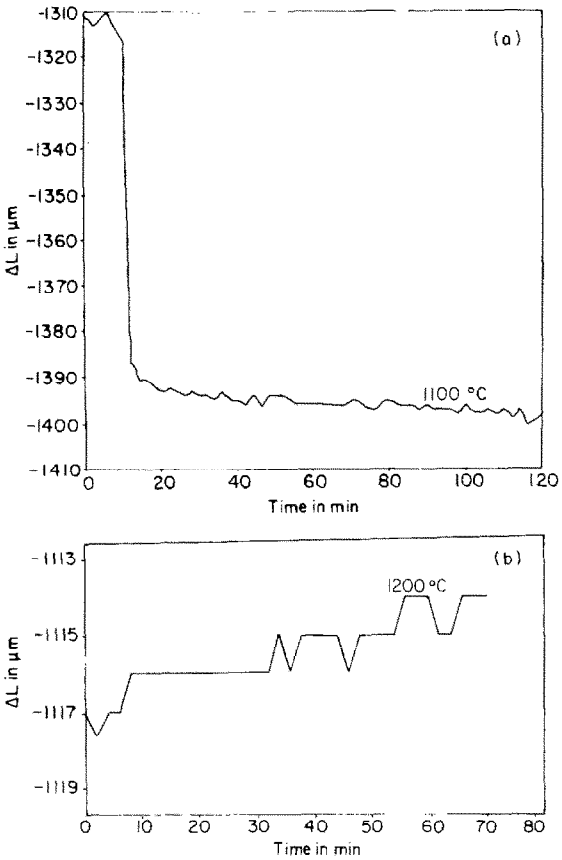

Fig. 7. a. Experimental isothermal TD curve (1100°C) for an $MnFe_2O_4$ sample compressed at 300 daN. b. Experimental isothermal TD curve (1200°C) for an $MnFe_2O_4$ sample compressed at 300 daN.

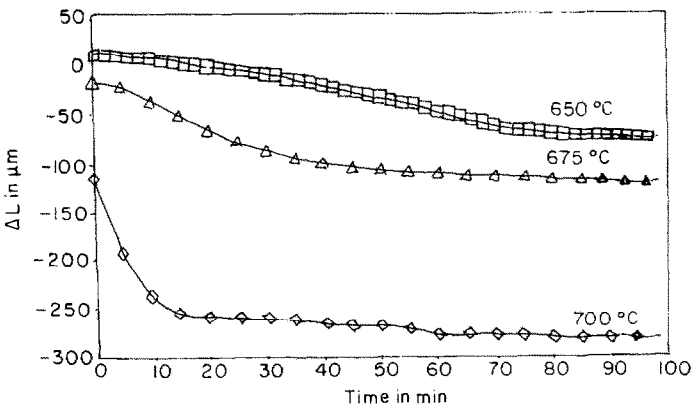

Fig. 8. Experimental isothermal TD curves for samples of $MnFe_2O_4$ compressed at 300 daN recorded in the temperature range 650–700°C.

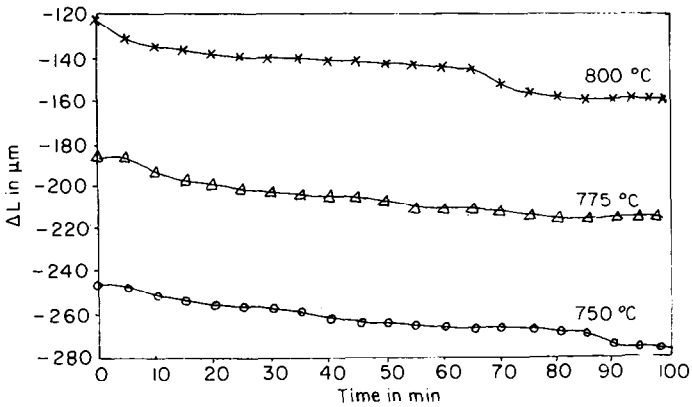

Fig. 9. Experimental isothermal TD curves for samples of $MnFe_2O_4$ compressed at 300 daN recorded in the temperature range 750–800°C.

By processing the TD curves (Figs. 8–12) according to the kinetic equations for the above-mentioned phenomena, we can show that in the range 650–800°C, the experimental data are described by the J.M.A.Y.K. equation [16]

$$\alpha = 1 - e^{-kt^n} \tag{2}$$

The results obtained for the temperature range are listed in Table 1.

At 650°C, the simple integral kinetic equation

$$\alpha = kt^n \tag{3}$$

also describes the experimental data, with $k = 7.2 \times 10^{-6}\ s^{-1.44}$, $n = 1.44$ and $r = 0.9979$. In our opinion, this is a consequence of the relatively low values

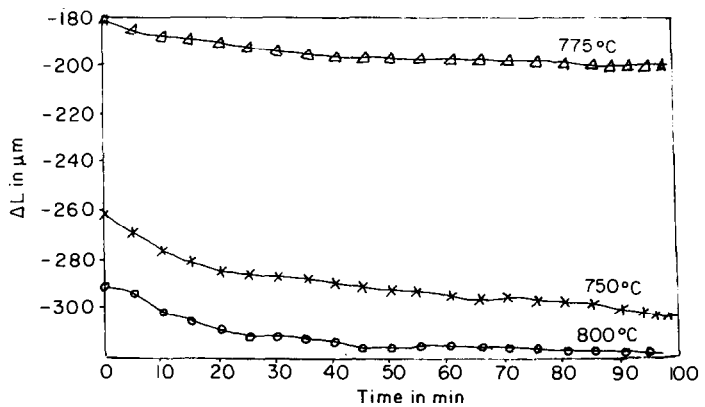

Fig. 10. Experimental isothermal TD curves for samples of $MnFe_2O_4$ compressed at 1000 daN in the temperature range 750–800°C.

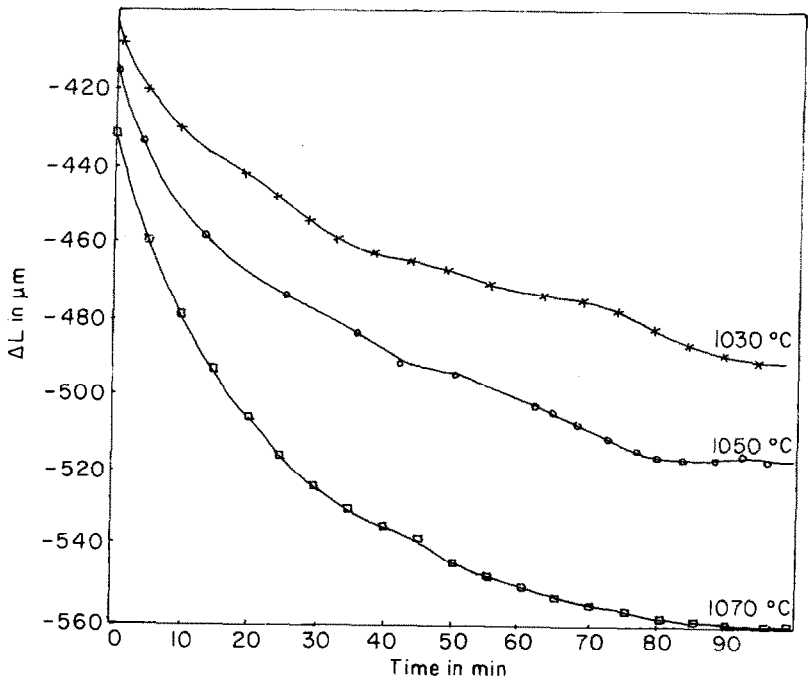

Fig. 11. Experimental isothermal TD curves for samples of $MnFe_2O_4$ compressed at 300 daN in the temperature range 1030–1070°C.

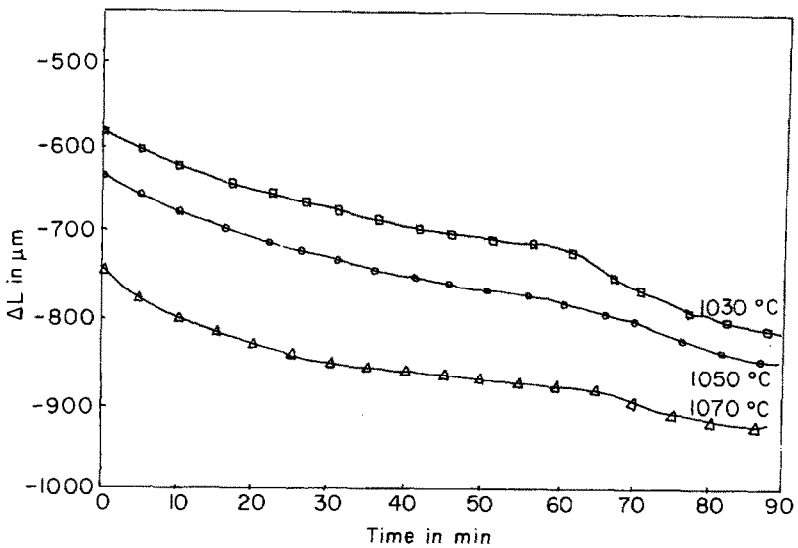

Fig. 12. Experimental isothermal TD curves for samples of $MnFe_2O_4$ compressed at 1000 daN in the temperature range 1030–1070°C.

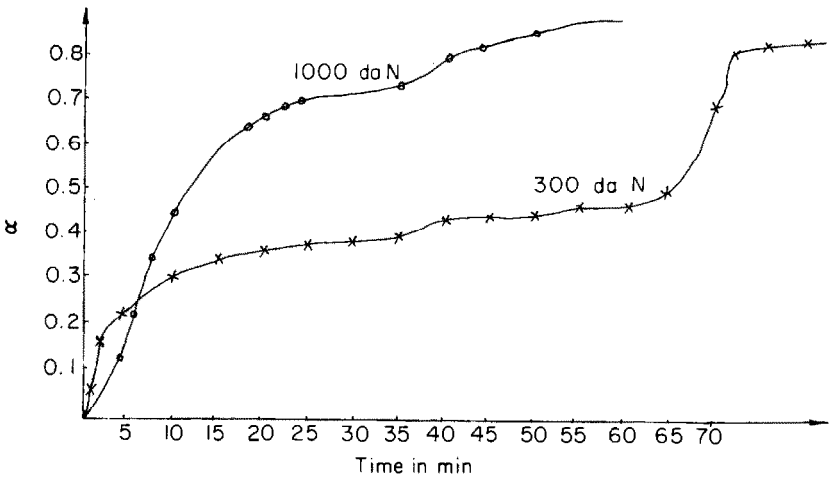

Fig. 13. Curves of isothermal conversion (750°C).

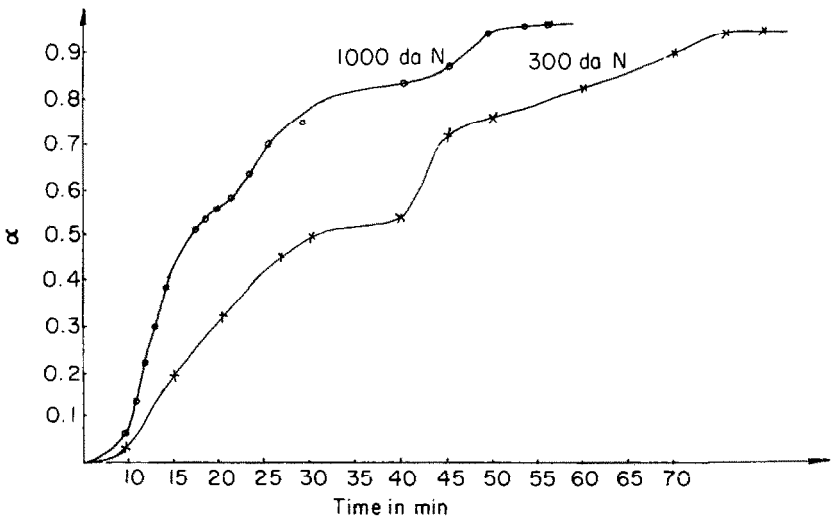

Fig. 14. Curves of isothermal conversion (800°C).

of α used to verify the equation. The logarithmic form of eqn. (2)

$$\ln(1-\alpha) = -kt^n \tag{4}$$

for low values of α, becomes

$$\alpha = kt^n \tag{5}$$

Thus, the fairly close values of k and n resulting from applying eqns. (2) and (3) are to be expected.

From Arrhenius plots ($\log k$, $1/T$), the following values of the pre-exponential factor and activation energy were obtained.

For the range 650–675°C (300 daN), $A = 9.75 \times 10^{9}\ s^{-1.55}$, $E = 66.8$ kcal mol^{-1}.

For the range 750–800°C (300 daN) $A = 3.41 \times 10^{21}\ s^{-1.51}$, $E = 125.8$ kcal mol^{-1}, $r = 0.9929$; (1000 daN) $A = 5.7 \times 10^{21}\ s^{-1.05}$, $E = 116.9$ kcal mol^{-1}, $r = 0.9989$.

Considering the significance of n in the J.M.A.Y.K. equation [16], and the values of n and of the activation energy obtained, the following mechanisms can be suggested for the temperature ranges indicated. For the range 650–675°C, in which the phases α-Fe_2O_3, Mn_2O_3 and Mn_3O_4 exist and continue to form, the values of n and E suggest a one-step nucleation with diffusional growth of nuclei. The values of n and k suggest a change in the mechanism at 700°C. For the range 750–800°C, in which solid solutions among the pre-existing Fe_2O_3, Mn_2O_3 and Mn_3O_4 phases are formed, the value $n \simeq 1$ (for 1000 daN) in the highly dispersed system indicates a surface nucleation characterised by an integral kinetic equation corresponding to a quasi-unity value of the "reaction order". Thus the interface process controls the nuclei growth and, in fact, the contraction step.

As can be seen from Table 2, in the range 1030–1070°C, the parabolic law $\alpha = kt^n$ describes the experimental data satisfactorily. (Strictly speaking, the parabolic law corresponds to $n = 0.5$.)

The following values were obtained for the Arrhenius parameters. At 300 daN: $\alpha \leq 0.60$, $A = 2.15 \times 10^{24}\ s^{-1.32}$, $E = 177.4$ kcal mol^{-1}, $r = 0.9987$; $0.47 \leq \alpha \leq 0.79$, $A = 4.78 \times 10^{36}\ s^{-0.74}$, $E = 240$ kcal mol^{-1}, $r = 0.9987$. At 1000 daN: $\alpha \leq 0.51$, $A = 1.2 \times 10^{4}\ s^{-1.26}$, $E = 51.9$ kcal mol^{-1}, $r = 0.9965$; $0.59 \leq \alpha \leq 0.96$, $A = 5.2 \times 10^{33}\ s^{-0.74}$, $E = 221.0$ kcal mol^{-1}, $r = 0.9904$.

According to the results obtained in the range 1030–1070°C, in which

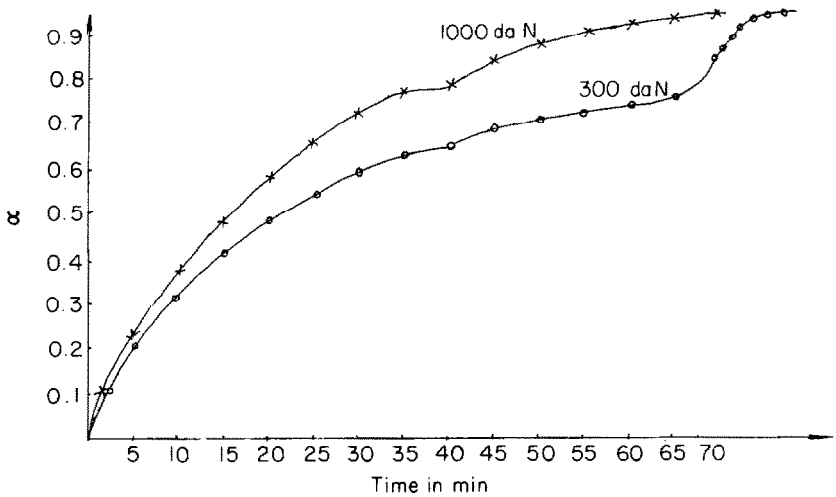

Fig. 15. Curves of isothermal conversion (1070°C).

TABLE 1

Values of the constant k and exponent n from eqn. (2) corresponding to the change undergone by $MnFe_2O_4$ compressed rings in the temperature range 650–800°C

300 daN	1000 daN
J.M.A.Y.K. equation	
650°C $\alpha = 0.12–0.42$ $n = 1.53$ $k = 2.92 \times 10^{-6}\ s^{-1.53}$ $r = 0.9962$	–
675°C $\alpha = 0.13–0.69$ $n = 1.58$ $k = 7.58 \times 10^{-6}\ s^{-1.58}$ $r = 0.9953$	–
700°C $\alpha = 0.2–0.855$ $n = 1.12$ $k = 1.80 \times 10^{-3}\ s^{-1.12}$ $r = 0.9970$	–
750°C $\alpha = 0.12–0.39$ $n = 1.59$ $k = 3.35 \times 10^{-6}\ s^{-1.59}$ $r = 0.9896$	$\alpha = 0.12–0.69$ $n = 1.08$ $k = 5.10 \times 10 \times 10^{-4}\ s^{-1.08}$ $r = 0.9895$
775°C $\alpha = 0.12–0.46$ $n = 1.48$ $k = 1.98 \times 10^{-5}\ s^{-1.48}$ $r = 0.9818$	$\alpha = 0.11–0.53$ $n = 0.96$ $k = 1.76 \times 10^{-3}\ s^{-0.96}$ $r = 0.9943$
800°C $\alpha = 0.10–0.50$ $n = 1.46$ $k = 6.01 \times 10^{-5}\ s^{-1.46}$ $r = 0.9921$	$\alpha = 0.13–0.56$ $n = 1.1$ $k = 7.5 \times 10^{-3}\ s^{-1.1}$ $r = 0.9908$

Key: r is the correlation coefficient of the linear regression.

$MnFe_2O_4$ is regenerated, the mass transfer at compaction occurs through parabolic bulk diffusion, with a change in mechanism during the isothermal treatment. According to the literature [8], the relatively high deviations with respect to the parabolic law recorded at 1070°C ($n = 0.33$ and respectively $n = 0.32$) could be attributed to the necks between crystalline grains. The melting along the grain boundaries at 1100°C, previously reported, confirms this statement.

TABLE 2

Values of the constant k and exponent n in the kinetic parabolic law $\alpha = kt^n$ corresponding to the change undergone by $MnFe_2O_4$ compressed rings in the range 1030–1070°C

300 daN	1000 daN
1030°C	
$\alpha = 0.1–0.35$	$\alpha = 0.14–0.51$
$n = 0.66$	$n = 0.66$
$k = 2.9 \times 10^{-6}\ s^{-1.32}$	$r = 0.9989$
$r = 0.9920$	$k = 2.12 \times 10^{-5}\ s^{-1.32}$
$\alpha = 0.47–0.7$	$\alpha = 0.59–0.83$
$n = 0.40$	$n = 0.43$
$k = 1.79 \times 10^{-4}\ s^{-0.80}$	$k = 3.7 \times 10^{-4}\ s^{-0.86}$
$r = 0.9908$	$r = 0.9987$
1050°C	
$\alpha = 0.07–0.39$	$\alpha = 0.1–0.68$
$n = 0.67$	$n = 0.61$
$k = 9.06 \times 10^{-6}\ s^{-1.34}$	$k = 3.0 \times 10^{-4}\ s^{-1.22}$
$r = 0.9937$	$r = 0.9931$
$\alpha = 0.506–0.69$	$\alpha = 0.7–0.85$
$n = 0.39$	$n = 0.36$
$k = 8.28 \times 10^{-4}\ s^{-0.78}$	$k = 1.0 \times 10^{-3}\ s^{-0.72}$
$r = 0.9975$	$r = 0.9953$
1070°C	
$\alpha = 0.18–0.60$	$\alpha = 0.2–0.77$
$n = 0.65$	$n = 0.63$
$k = 2.25 \times 10^{-5}\ s^{-1.30}$	$k = 3.9 \times 10^{-5}\ s^{-1.26}$
$r = 0.9973$	$r = 0.9968$
$\alpha = 0.66–0.79$	$\alpha = 0.8–0.96$
$n = 0.33$	$n = 0.32$
$k = 2.85 \times 10^{-3}\ s^{-0.66}$	$k = 4.8 \times 10^{-3}\ s^{-0.64}$
$r = 0.9954$	$r = 0.9903$

CONCLUSIONS

In the temperature range 650–1100°C, which is characteristic for most of the compaction, the sintering of $MnFe_2O_4$ occurs in a homogenous multi-component system with superimposed solid state reactions. In the same temperature range, the sintering of $MnFe_2O_4$ occurs mainly in three distinct steps with specific kinetics and mechanisms for three narrower temperature ranges.

REFERENCES

1 L.M. Letjuk and G.J. Zuravlev, Chemistry and Technology of Ferrites, (in Russian), Khimiya, Leningrad, 1983, pp. 81, 226, 231.
2 R.M. German, Sintering—New Developments, Proc. 4th Int. Round Table Conf. on Sint., Dubrovnik, Yugoslavia, Sept. 5–10, 1977, p. 18.

3 J. Šestak, V. Šatava and W.W. Wendlandt, Thermochim. Acta, 7 (1973) 432.
4 I. Sitidze and H. Sato, Ferrites (in Russian), Mir, Moscow, 1964, p. 112.
5 G.C. Kuczynski, Sintering and Related Phenomena, Proc. 2nd Conf. Sint. Rel. Phen., Notre Dame, 1966, Gordon and Breach, New York, 1967, p. 685.
6 G.C. Kuczynski, Reactivity of Solids, 5th Int. Symp. Reactivity of Solids, Elsevier, Amsterdam, 1965, p. 352.
7 D.A. Venkatu and G.C. Kuczynski, Kinetics of Reactions in Ionic Systems, Materials Science Research, Vol. 4, Plenum Press, London, 1969, p. 316.
8 G.C. Kuczynski, Ferrites, Proc. Int. Conf. (Japan), July 1975, p. 87.
9 A.D. Smigelskas and E.O. Kirkendall, Trans. AIME, 171 (1947) 130.
10 G.S. Hartley, Trans. Faraday Soc., 42 (1946) 6.
11 M. Paulus, Ferrites, Proc. Int. Conf. (Japan), July 1970, p. 114.
12 T. Akashi, J. Sugano and T. Okuda, Ferrites, Proc. Int. Conf. (Japan), July 1970, p. 96.
13 H.L. Turk, Ferrites, Proc. Int. Conf. (Japan), July 1970, p. 99.
14 A.L. Stuijts, Ferrites, Proc. Int. Conf. (Japan) July 1970, p. 108.
15 M. Ito, M. Senna and H. Kun, Ferrites, Proc. Int. Conf. (Japan), Sept.–Oct. 1980, p. 50.
16 I.G. Murgulescu, T. Oncescu and E. Segal, Introducere in Chimia-Fizica, (in Romanian), Vol. II, 2nd edn., Academiei, Bucharest, 1981, p. 701, 742.
17 E.N. Yeremin, The Foundations of Chemical Kinetics, Mir, Moscow, 1979, pp. 56, 59, 382.
18 H. Schumann, Metalografie, Ed. Technica, Bucharest, 1962, p. 79.